Density-functional theory for structure and freezing of star polymer solutions

Benito Groh[a)]
FOM Institute for Atomic and Molecular Physics, Kruislaan 407, 1098 SJ Amsterdam, The Netherlands

Matthias Schmidt
Institut für Theoretische Physik II, Heinrich-Heine-Universität Düsseldorf, Universitätsstraße 1, D-40225 Düsseldorf, Germany

(Received 10 October 2000; accepted 21 December 2000)

We use the soft fundamental measure theory (SFMT) to investigate a system of classical particles interacting with the pair potential of star polymers in solution. To that end we calculate liquid and solid structural properties, as well as freezing, solid-to-solid, and remelting phase transitions. Even subtle physical effects, like deviations from Gaussian crystal peaks and an anomalous peak broadening upon increasing density as well as a reasonable vacancy concentration are captured correctly. Good overall quantitative agreement with simulation data is found, however, with a tendency to overestimate the structural correlations. Furthermore, we demonstrate that all recent developments of its hard core counterpart can be incorporated systematically into SFMT. © *2001 American Institute of Physics.* [DOI: 10.1063/1.1349092]

I. INTRODUCTION

The understanding of classical many-body systems has received a boost by the development of density functional theory (DFT).[1] The density functional of a given system is an extremely powerful object, from which a complete understanding of an equilibrium system can be gained. The thermodynamics and correlation functions up to an arbitrary order are accessible in principle. Moreover, this is not only true for the bulk but also for situations where an arbitrary influence that can be modeled by an external potential energy, is acting on the system. Apart from externally caused spatial inhomogeneities, DFT also accounts for self-sustained density-waves that are present in a crystal. Thus, it is able to describe the liquid and solid phases on an equal footing, and hence gives a physical explanation of the existence of the freezing phase transition.

As the free energy density functional (DF) is such a powerful object, it may become obvious that it is unknown for most realistic systems. To construct an approximation to the exact DF, the common strategy is to require that the approximative DF yields the correct behavior in situations where one can solve the system, at least approximatively. The more conventional approach uses the homogeneous liquid phase as this starting point, and requires that the approximative DF reproduces known results from liquid state theory, like the equation of state and correlation functions. These quantities can be considered as *input* to the theory.

A newer approach utilizes situations of reduced spatial dimensionality as limiting cases that are captured correctly. There one has the advantage that the system can be solved exactly in dimensions as low as one or even zero, so no approximations enter at that stage. The Rosenfeld hard-sphere functional[2] can be derived in this way,[3] and improved versions of it can be systematically obtained,[4,5] as well as functionals for parallel hard cubes.[6,7] The approximation one has to do is to construct a ''functional interpolation'' [5] between spatial dimensions. The fundamental measure functionals yield the Percus–Yevick direct correlation function and equation of state for the bulk hard sphere liquid, give excellent results for the coexistence densities and describe the crystal structure up to close-packing excellently,[8] as well as the vanishingly small vacancy concentration.[9] We note that recently a similar approach was used to find a DFT for adhesive hard spheres.[10]

The idea that a three-dimensional functional can be constructed by imposing its correct dimensional crossover to lower dimensions is not limited to hard interactions. It can be applied to penetrable spheres,[11,12] the Asakura–Oosawa colloid-ideal polymer mixture,[13] and has been exploited to derive a DFT for arbitrary soft pair interactions[14,15] and additive mixtures.[16] This so-called soft fundamental measure theory (SFMT) was demonstrated to predict the properties of the homogeneous liquid phase. The fluid equation of state and pair correlation function are an *output* of the theory.

In this work we apply the SFMT to a system of star polymers in a good solvent, which has attracted a lot of recent interest.[17–22,24,25] The logarithmic pair interaction[17] present in this system leads to an anomalous liquid structure[18] and to a rich phase diagram[19,20] with various solid phases and reentrant melting upon increasing density. Pair[21] and triplet[22] interactions have been investigated. Besides computer simulations, liquid integral equations[17,18] and Einstein-crystal perturbation theory[19,20] have been employed. It is of great interest to investigate the system from the unifying viewpoint that DFT provides. In addition, because of the richness of physical phenomena, star polymers provide a severe test to any DFT.

[a)]Current address: Fachbereich Physik, Bergische Universität Wuppertal, D-42097 Wuppertal, Germany.

Our results show that the SFMT stands this test. In particular, the predicted bulk pair correlations are in good agreement with simulations over the whole range from hard-sphere-like to ultrasoft behavior. The DFT yields thermodynamically stable face-centered cubic (fcc) and body-centered cubic (bcc) crystals and reentrant melting. We find that the lattice peaks have broader wings than Gaussians. A peculiar decreasing of the Lindemann parameter upon increasing the density is captured correctly.

In Sec. II the SFMT functional is described. We also give its refinements according to the latest developments in FMT for hard spheres, and discuss briefly its properties. Section III defines the theoretical model for star polymer solutions and gives explicit expressions for the quantities involved in SFMT. In Sec. IV we present results for the liquid and solid structure as well as the phase diagram. The present approach is discussed in the concluding Sec. V.

II. THE DENSITY FUNCTIONAL

A. Definition

The SFMT is a weighted density approximation. It employs a set of weight functions which are independent of the density profile. The free energy density is a function of the weighted densities and is analytically given.

The excess free energy is expressed as

$$F^{\mathrm{exc}}(T,[\rho(\mathbf{r})])=k_BT\int d\mathbf{x}\Phi(\{n_\alpha(T,\mathbf{x})\}), \tag{1}$$

where T is the temperature, and k_B is Boltzmann's constant. The integrand is a reduced free energy density Φ depending on a set of weighted densities $\{n_\alpha\}$ indexed by α. Each weighted density is given by a convolution of its temperature-dependent weight function w_α with the density profile,

$$n_\alpha(T,\mathbf{x})=\int d\mathbf{r}\rho(\mathbf{r})w_\alpha(T,\mathbf{x}-\mathbf{r}). \tag{2}$$

Within the set of weight functions there is a hierarchy,

$$w_2(r)=-\frac{\partial w_3(r)}{\partial r}, \tag{3}$$

$$\mathbf{w}_{v2}(r)=w_2(r)\mathbf{r}/r, \tag{4}$$

$$\hat{\mathbf{w}}_{t2}(r)=\mathbf{w}_{v2}(r)\mathbf{r}/r, \tag{5}$$

$$w_1(r)=w_2(r)/(4\pi r), \tag{6}$$

$$\mathbf{w}_{v1}(r)=w_1(r)\mathbf{r}/r, \tag{7}$$

$$w_0(r)=w_1(r)/r, \tag{8}$$

where w_2, w_1, w_0 are scalar quantities, $\mathbf{w}_{v1}$, $\mathbf{w}_{v2}$ are vectors, and $\hat{\mathbf{w}}_{t2}$ is a second rank tensor given by a dyadic product of a vector density and a unit spatial vector. The introduction of the tensorial weight $\hat{\mathbf{w}}_{t2}$ is justified below. The ''generating'' weight function w_3 is determined so that a deconvolution of the Mayer bond $f(r)=\exp[-\beta V(r)]-1$, where $\beta=1/k_BT$, is generated,

$$-\tfrac{1}{2}f(r)=w_0*w_3+w_1*w_2-\mathbf{w}_{v1}*\mathbf{w}_{v2}, \tag{9}$$

where the convolution product, denoted by $*$, also implies scalar products between vectors.

The free energy density is given by $\Phi=\Phi_1+\Phi_2+\Phi_3$, with the contributions

$$\Phi_1=-n_0\ln(1-n_3), \tag{10}$$

$$\Phi_2=\frac{n_1n_2-\mathbf{n}_{v1}\cdot\mathbf{n}_{v2}}{1-n_3}. \tag{11}$$

The third term exists in various refined forms,

$$\Phi_3^{\mathrm{FMT1}}=\frac{1}{24\pi}\frac{n_2^3(1-(\mathbf{n}_{v2}/n_2)^2)^3}{(1-n_3)^2}, \tag{12}$$

$$\Phi_3^{\mathrm{FMT2}}=\frac{9}{8\pi}\frac{\det\hat{\mathbf{n}}_{t2}}{(1-n_3)^2}, \tag{13}$$

$$\Phi_3^{\mathrm{FMT3}}=\frac{\mathbf{n}_{v2}\cdot\hat{\mathbf{n}}_{t2}\cdot\mathbf{n}_{v2}-n_2\mathbf{n}_{v2}\cdot\mathbf{n}_{v2}-\mathrm{tr}(\hat{\mathbf{n}}_{t2}^3)+n_2\,\mathrm{tr}(\hat{\mathbf{n}}_{t2}^2)}{(16\pi/3)(1-n_3)^2}, \tag{14}$$

where tr denotes the trace, and det is the determinant of a second-rank tensor.

FMT1 (Ref. 3) is the form that first gave a freezing transition for hard spheres and was used in the proposal of SFMT[14] FMT2 (Ref. 8, 4) produces a far better description of the hard sphere solid, but gives less accurate direct correlations for the liquid. FMT3 (Ref. 5) is the latest improvement combining the power of both ancestors. Each of these forms is taken over from the corresponding hard sphere functional. Our modification is the replacement of the hard sphere weight functions with those for the soft potential. This requires the introduction of a tensorial soft weight, done in Eq. (5). The form of $\hat{\mathbf{w}}_{t2}$ is unique in the current framework. This can be seen as follows. The numerator of Φ_3^{FMT2} and Φ_3^{FMT3} is of third order in weighted densities. Hence a single weighted density has to have the dimension of inverse length to give an overall inverse volume, which is the dimension of the free energy density. Hence the tensorial weight carries the index $t2$. The simplest way to construct such a weight function, so that the hard sphere case is respected, is by multiplying $\mathbf{w}_{v2}$ by a spatial unit vector, and Eq. (5) is obtained.

B. Properties

The density functional defined above is exact in two extreme limiting cases, the zero-dimensional (0D) and the low-density limit. The 0D limit is a an extremely confined situation, represented by $\rho(\mathbf{r})=\eta\delta(\mathbf{r})$. We note that as the excess free energy functional does not depend on the external potential V_{ext}, there is no need to specify a V_{ext} that causes the 0D distribution. Nevertheless it might be useful to think of a small cavity that immobilizes a particle. There can be at most one particle, because the pair interaction diverges at the origin. The free energy can be calculated exactly.[3] The SFMT reproduces this solution.[14]

In the low-density limit, the functional becomes exact up to second order in the virial expansion. The reason is that the weight functions restore the Mayer function upon convolution. Details of the calculation can be found in Ref. 14.

III. STAR POLYMERS

Star polymers are macromolecular entities consisting of a functional center to which f polymeric arms are attached. The arm-number or functionality f is an integer ranging from 2 to values as high as 256. When soluted in a good solvent, star polymers can be regarded as colloidal particles on a mesoscopic length scale, that is much larger than the microscopic scale of individual monomers building up the arms. The colloidal picture involves an effective pair[21] or even triplet[22] interaction between the stars, which arises from entropic effects due to reduction of the number of accessible states if the stars are very close to each other. The resulting interaction is repulsive with a logarithmic law. For large distances it decays faster and a hybrid between logarithmic and a Yukawa form was proposed[17] and validated by simulations.[21] The arm-number governs the softness ranging from ultra-soft for small f to practically hard spheres for large f.

A. The potential

As a model interaction between star polymers we use the modified potential of Ref. 14 given by

$$\beta V(r)=\begin{cases} -2q\ln(r/R)+\ln\binom{2q}{q} & 0\leqslant r<R \\ \phi_q(r)+\ln\binom{2q}{q} & R\leqslant r<2R \\ 0 & 2R\leqslant r \end{cases}, \tag{15}$$

where $\binom{2q}{q}$ is the binomial coefficient. The crossover function between small and large distances is given by

$$\phi_q(r)=-\ln[(1+\xi)^{2q}-\xi^{q+1}B_{q\,2} \times F_1(1,1-q;2+q;-\xi)], \tag{16}$$

where $\xi=(r/R)-1$, $B_q=2\Gamma(1+2q)\Gamma^{-1}(q)\Gamma^{-1}(2+q)$, Γ is the Euler gamma function, and ${}_2F_1$ is the hypergeometric function. For integer q the crossover function can be simplified to a polynomial, $\phi_q(r)=-\ln[(1+\xi)^{2q}-\Sigma_{j=0}^{q}\binom{2q}{j}\xi^q]$. The parameters q and R are related to the arm-number f and length scale σ of the log-Yukawa potential[17] via $q=(5/36)f^{3/2}$, and $R/\sigma=\exp[(1+\sqrt{f}/2)^{-1}-(2q)^{-1}\ln\binom{2q}{q}]$. We define a dimensionless density $\rho^*=(2R)^3N/V$. The relation $\eta^*=(\pi/6)(2R/\sigma)^{-3}\rho^*$ holds, where η^* is the density of Ref. 17.

The log-hypergeometric form (15) for the potential is not chosen on physical grounds. It only simplifies the actual calculations, because the weight functions can be obtained analytically. This makes the numerical work easier, as no inaccuracies enter at that stage. We plot both interactions in Fig. 1. The force $F=-dV/dr$ as well as the potential itself are shown for both functional forms and are compared to the simulation data by Jusufi *et al.*[21,26] Both functions are mathematically identical for $r/R<1$. On the scale of the plot, however, both forces coincide for larger distances up to $r/R\approx 1.5$, where the cusp in the log-Yukawa force appears. The cusp is absent in the present case of the hypergeometric crossover. However, it falls off too quickly for larger distances and even vanishes for $r/R>2$. There the simulations indicate a finite force that is well described by the log-Yukawa potential. Nevertheless, we conclude that the gross features are the same for both models and the use of the log-hypergeometric potential is justified for our investigations.

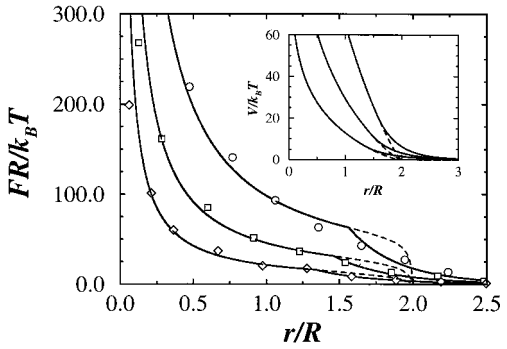

FIG. 1. Comparison of two functional forms for the star polymer pair interactions. The main plot shows the scaled force $FR/(k_BT)$, the inset indicates the scaled potential $V/(k_BT)$ itself. Both are plotted as a function of the scaled distance r/R. The solid lines represent the log-Yukawa potential by Likos *et al.* (Ref. 17), the dotted lines indicate where the log-hypergeometric potential used in this work differs. The symbols are the computer simulation results by Jusufi *et al.* (Ref. 21), Fig. 3(b) therein (Ref. 26). From top to bottom the arm number changes as $f=50, 30, 18$, corresponding to $q=49.1, 22.8, 10.6$.

B. Setting up the density functional

The weight functions for star polymers are obtained by solution of the deconvolution Eq. (9), and are explicitly given by

$$w_3(r)=\theta(R-r)[1-(r/R)^q], \tag{17}$$

$$w_2(r)=\theta(R-r)qr^{q-1}/R^q, \tag{18}$$

$$\mathbf{w}_{v2}(r)=\theta(R-r)[qr^{q-1}/R^q]\hat{\mathbf{r}}, \tag{19}$$

$$\hat{\mathbf{w}}_{t2}(r)=\theta(R-r)[qr^{q-1}/R^q]\hat{\mathbf{r}}\hat{\mathbf{r}}, \tag{20}$$

$$w_1(r)=\theta(R-r)qr^{q-2}/(4\pi R^q), \tag{21}$$

$$\mathbf{w}_{v1}(r)=\theta(R-r)[qr^{q-2}/(4\pi R^q)]\hat{\mathbf{r}}, \tag{22}$$

$$w_0(r)=\theta(R-r)qr^{q-3}/(4\pi R^q), \tag{23}$$

where $\hat{\mathbf{r}}=\mathbf{r}/r$ is a unit vector, and θ is the Heaviside step function. The weight functions do not depend on temperature, because the pair interaction, Eq. (15), is of entropic origin, hence $V(r)/k_BT$ is constant with respect to temperature. As a quasithermodynamic quantity the softness parameter q tunes the shape of the interaction and of the weight functions.

C. Computer simulation

To provide data for comparison with the DFT results, we have carried out Monte Carlo (MC) computer simulations of the log-hypergeometric pair potential, Eq. (15). Canonical simulations with 108–864 particles and 10^5-10^6 MC moves per particle were performed. We collect data for the pair correlation function in the fluid state and crystal density dis-

tributions. For the latter the usual subtraction of the center-of-mass movement was done. The actual data presented are from a system with 256 particles. We checked that the finite size dependence is negligible at one state point, $q=100$, $\rho^*=\sqrt{2}$.

IV. RESULTS

A. Liquid structure

The SFMT has the ability to *predict* the properties of the homogeneous liquid. The thermodynamics and correlation functions can be derived from the functional and are not put in by hand, say from liquid state theory. In the following, we calculate the bulk liquid free energy and pair distribution functions. The latter are compared to simulations.

For a liquid state with homogeneous density $\rho(\mathbf{r})=\rho$, the weighted densities become $n_\alpha=\xi_\alpha\rho$, where the soft fundamental measures ξ_α are given by $\xi_\alpha=4\pi\int_0^\infty dr r^2 w_\alpha(r)$. We obtain $\xi_\alpha=\xi_\alpha^{\mathrm{HS}}q/(q+\alpha)$, where the fundamental measures of a hard sphere of radius R are the Euler characteristic $\xi_0^{\mathrm{HS}}=1$, integral mean curvature $\xi_1^{\mathrm{HS}}=R$, surface area $\xi_2^{\mathrm{HS}}=4\pi R^2$, and volume $\xi_3^{\mathrm{HS}}=4\pi R^3/3$. For the star polymers the Euler characteristic remains unity, $\xi_\alpha=1$, the other fundamental measures are $\xi_1=Rq/(q+1)$, $\xi_2=4\pi R^2 q/(q+2)$, $\xi_3=(4\pi/3)R^3 q/(q+3)$. We emphasize that the flexibility contained in ξ_α, $\alpha=1,2,3$ cannot be obtained by a mapping onto a reference hard sphere system.

The vector densities vanish, $\mathbf{n}_{v1}=\mathbf{n}_{v2}=0$, and $(\hat{\mathbf{n}}_{t2})_{ij}=\delta_{ij}n_2/3$. The excess free energy is

$$\frac{\beta F^{\mathrm{exc}}}{V}=-n_0\ln(1-n_3)+\frac{n_1 n_2}{1-n_3}+\frac{n_2^3}{24\pi(1-n_3)^2} \qquad (24)$$

in all three approximations for Φ_3. The liquid equation of state is easily derived by differentiation and reduces to the hard sphere Percus–Yevick compressibility result for $q\to\infty$.

To calculate pair correlations from a density functional there are various ways to go. They differ in the number of *test particles* that one inserts. A test particle corresponds to an external potential coinciding with the pair potential itself. For one test particle the pair correlations are proportional to the density profile itself. This is a widely used approach; the profile depends on the radial coordinate. Without a test particles, $g(r)$ can be computed via the direct correlation function given by the second functional derivative of the excess free energy using the Ornstein–Zernike relation. We employ this strategy because we consider it as the tougher test for the functional itself, as no oscillating density profile is minimized.

We will investigate the crossover behavior of the pair correlations from soft to hard sphere behavior for the density $\rho^*=3/\pi=0.955$. The ultrasoft case, $q=3$, was already considered in Ref. 14. In Fig. 2 the theoretical results are shown together with simulation data for different softness parameters $q=6,12,24$. We observe that the phase and amplitude of the oscillations are reproduced nicely by the DFT. The only deficiencies are an overshooting of the first peak for $q=6$ and negative values for small distances for all q. On physical grounds, these values may be disregarded, as $g(r)$ is a non-negative function. They present a shortcoming of the current approach, but incorporating the feature $g(r)\geqslant 0$ on the level of the density functional itself is not an easy task. Of course, one could get rid of the negative values using the test-particle method where the ideal gas free energy ensures non-negative results.

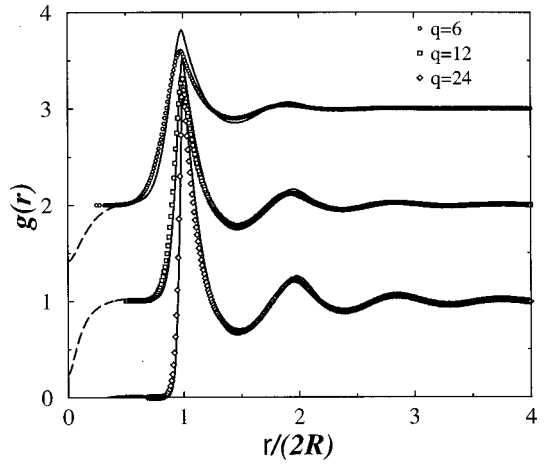

FIG. 2. Pair distribution function $g(r)$ as a function of the scaled distance $r/(2R)$. Results for various softness parameters are shown, $q=6, 12, 24$ (from top to bottom) and density $\rho^*=3/\pi=0.955$. The lines are the DFT results, the symbols are Monte Carlo data. The curves are shifted upwards one unit for reasons of clarity. For small distances the theoretical result becomes negative (indicated by a dashed line).

B. Solid structure

A general crystalline density has the form,

$$\rho(\mathbf{r})=\sum_{\mathbf{R}}\rho_\Delta(\mathbf{r}-\mathbf{R}) \qquad (25)$$

with identical lattice peaks $\rho_\Delta(\mathbf{r})$ centered at the lattice sites $\{\mathbf{R}\}$. A corresponding decomposition is induced for the weighted densities,

$$n_\alpha(\mathbf{r})=\sum_{\mathbf{R}} n_\Delta^{(\alpha)}(\mathbf{r}-\mathbf{R}) \qquad (26)$$

with

$$n_\Delta^{(\alpha)}(\mathbf{r})=\int d^3r'\rho_\Delta(\mathbf{r}')w_\alpha(\mathbf{r}-\mathbf{r}'). \qquad (27)$$

In the following we assume spherical density peaks $\rho_\Delta(\mathbf{r})=\rho_\Delta(r)$, but, for the time being, do not restrict their shape further, in contrast to the common approximation by Gaussians.[1] For the scalar weight functions this leads to

$$n_\Delta^{(\alpha)}=\frac{2\pi}{r}\int_0^\infty dr' r'\rho_\Delta(r')\int_{|r-r'|}^{r+r'} dr_{12} r_{12} w_\alpha(r_{12}). \qquad (28)$$

Since the second integral can easily be performed for our polynomial weight functions only a one-dimensional numerical integration is necessary to compute the weighted densities. Similar, slightly more complex expressions result for the vector and tensor weighted densities.

Usually $\rho_\Delta(r)$ is zero (or negligible small) for distances r beyond a cutoff r_c, which implies an upper cutoff for

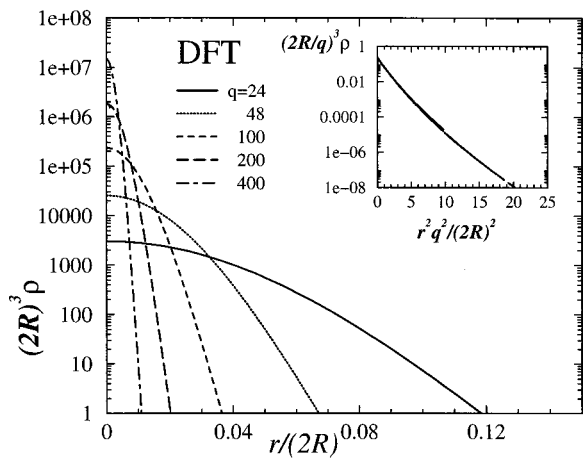

FIG. 3. Density functional results for the density peaks in an fcc crystal as a function of the distance r from the lattice site. Results for different softness are shown, $q=24, 48, 100, 200, 400$; at the density $\rho^*=\sqrt{2}$ corresponding to a close-packed hard-sphere ($q\to\infty$) crystal. Note the logarithmic ordinate extending over eight decades in density. The inset shows the same data scaled as $(2R/q)^3\rho$ as a function of the scaled and squared distance $r^2q^2/(2R)^2$.

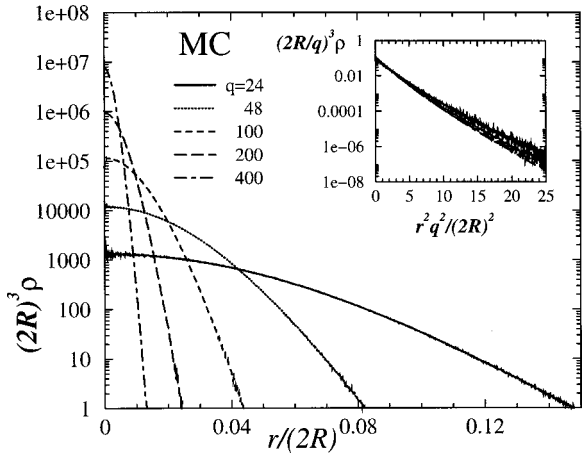

FIG. 4. Same as Fig. 3, but obtained from Monte Carlo computer simulations.

$n_\Delta^{(\alpha)}(r)$ at $r=R+r_c$. (In contrast to the hard sphere case there is no lower cutoff.) Therefore only a few lattice sites **R** contribute in Eq. (26) to the full weighted densities at any point. For the determination of the free energy we have employed two different numerical methods, depending on the width of the density profile. Method I applies to narrow profiles, for which only either one or two lattice sites contribute at every point. By taking advantage of the resulting symmetries the integration in Eq. (1) can be reduced to a one- and a two-dimensional numerical integral. Details can be found in Ref. 8. In method II we perform a full three-dimensional integration over an asymmetric unit, i.e., the smallest region with which space can be filled by applying the space group symmetries. For fcc and bcc crystals this corresponds to 1/48 of the Wigner–Seitz cell. For a given profile width we first make a list of the relevant lattice sites whose distance to the integration region is smaller than $R+r_c$. This approach fails for too narrow peaks because then the integration routine cannot reliably sample the integrand which takes on considerable values only in a narrow quasi-two-dimensional subset of the integration region.

The functional derivative $\delta F^{\rm exc}/\delta\rho(r)$ is determined as demonstrated for hard spheres in Ref. 8, using analytical expressions for $\delta n_\Delta^{(\alpha)}(r')/\delta\rho_\Delta(r)$ and the same integration method as for the functional itself. In order to solve the stationarity equation

$$\rho_\Delta(r)=\frac{\exp\{-(1/4\pi r^2)\,\delta f^{\rm exc}/\delta\rho_\Delta(r)\}}{4\pi\int dr'\,r'^2\exp\{-(1/4\pi r^2)\,\delta f^{\rm exc}/\delta\rho_\Delta(r')\}} \tag{29}$$

with $f^{\rm exc}=\beta F^{\rm exc}/N$ the profile is discretized over a mesh in r. Then Eq. (29) is iterated starting from a reasonable initial guess until the maximum relative change of $\rho_\Delta(r)$ in one iteration is less than 10^{-5}.

In Fig. 3 we show the results for different softness parameters q at a fixed density $\rho^*=\sqrt{2}$, equal to the close packing density for hard spheres. As expected the profiles become wider when the interaction potential softens. The *shape* remains essentially the same; if distance is scaled by q (and correspondingly density by q^{-3}) all curves practically coincide, as shown in the inset. Using a logarithmic plot of ρ vs r^2 moreover demonstrates that the peaks are almost Gaussian but have wider wings than a Gaussian fitted to the central part. In Fig. 4 we provide a direct comparison with computer simulations for the same parameters. They exhibit the same scaling behavior, but are slightly narrower (about 30%). Even the deviations from the Gaussian shape agree with the density-functional result. Note that strictly speaking, simulation and theoretical profiles differ in the following respect. The theoretical profiles minimize the DFT, if radially symmetric profiles are assumed. In principle, this is different from a spherical average of the minimizing profile with angular anisotropy. In the simulation, clearly, the equivalent of the latter is obtained. The difference, however, is expected to be small, because anisotropy of lattice sites is small (see, e.g., Ref. 23 for hard sphere results).

Here and in the following we always used the most advanced DFT version FMT3. We checked one state point ($\rho^*=1.4127$, $q=100$) for the older versions. The peak width is measured by

$$w=\left[\frac{8\pi}{3}\int_0^\infty dr\,r^4\rho_\Delta(r)\right]^{1/2} \tag{30}$$

so that for Gaussian peaks

$$\rho_\Delta(r)=\frac{1}{\pi^{3/2}w^3}\exp[-(r/w)^2]. \tag{31}$$

It differs only by 5% between FMT3 and FMT2, whereas the FMT1 result is narrower by a factor 5. Also the shapes are very similar for the first two cases, but a peculiar long tail arises in FMT1.

In Fig. 5 we present the dependence of the profile width on the nearest neighbor distance $R_{nn}=2R(\sqrt{2}/\rho^*)^{1/3}$ in an fcc crystal with $q=100$. The lower and upper part of the solid line are obtained by methods I and II, respectively. There is no overlap range where both methods can be ap-

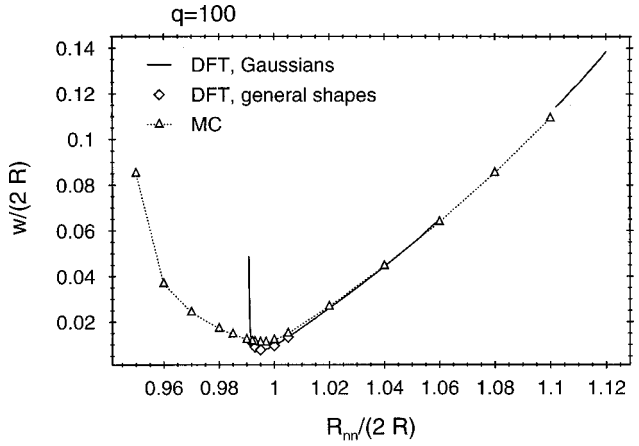

FIG. 5. Dependence of the width of the crystalline peaks [as defined in Eq. (30)] on the nearest neighbor distance in a fcc solid for $q=100$. The solid line is the DFT result assuming a Gaussian peak shape, obtained with methods I (lower part) and II (upper part) described in the text. The diamonds are obtained by the minimization with radially symmetric peaks. The triangles are Monte Carlo data.

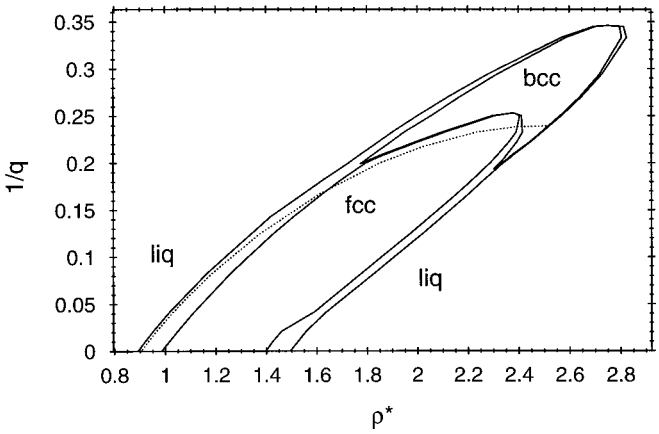

FIG. 6. Phase diagram of star polymers obtained by density functional theory as a function of the density ρ^* and the inverse softness parameter q^{-1}. All phase transitions are first order. The dotted line indicates the estimate of the freezing density by the Hansen–Verlet criterion.

plied, but the results connect nicely with each other. In both cases Gaussian profiles [Eq. (31)] were assumed. The widths from the radial minimization, indicated by diamonds, are not distinguishable from the Gaussians on the scale of the figure. Upon compression from the low density side the peaks first become narrower. However, just above $R_{nn}=2R$ surprisingly the width increases again. This increase is found both in simulation and theory, but is much steeper in DFT. The same behavior occurs for smaller q, even for the bcc crystal, but the minimum shifts towards higher R_{nn} and larger widths w.

The occurrence of vacancies can be taken into account within DFT by allowing non-normalized density peaks, i.e., less than one particle per lattice site on average, and treating the normalization constant as an additional minimization parameter. The FMT is the first DFT for which this procedure yields reasonably small vacancy concentrations[9] for hard spheres.

Determining the average occupancy number in this way for star polymers, we find that SFMT also predicts almost normalized density peaks. There is a tiny negative vacancy concentration of the order of 10^{-5} near melting. This would mean that there are more double occupied sites than empty ones. Whether this is an artifact of the DFT or a feature of the peculiar logarithmic interaction of star polymers remains an open question.

C. The phase diagram

In order to compute the phase diagram of our star polymer model we determined the free energy in the Gaussian approximation for a large number of densities and softness parameters. Phase coexistence densities then follow by the usual common tangent construction. Our results are displayed in Fig. 6. For relatively hard interactions the fluid freezes into an fcc crystal, for soft interactions ($q\lesssim 4$) into a bcc crystal. Upon further compression both crystals eventually remelt. The broadening of the profile discussed in the previous section is a precursor of this remelting transition. Note that formally hard spheres ($q=\infty$) also remelt, because the solid but not the liquid free energy diverges at close packing. However, in this case the coexistence region extends into the unphysical density range beyond close packing. It must be stated that the present DFT has intrinsic limitations at high density. Any density distribution, where locally $n_3>1$ is punished by an infinite energy cost. In reality, such distributions will have large, but finite free energy.

In an intermediate softness range both fcc and bcc solids occur with the sequence liquid–fcc–bcc–fcc–liquid. The dotted line denotes the points where the main peak of the liquid structure factor reaches the value 2.8. This has been suggested as a general phenomenological freezing criterion by Hansen and Verlet[27] and lies close to the actual phase transition for not too small q. This demonstrates the internal consistency of the theory. For $q\lesssim 2.9$ the solid phase disappears completely.

Freezing and remelting of star polymers have been theoretically predicted before[28] and were observed experimentally in the closely related system of diblock copolymer micelles.[29,30] In the latter work bcc was observed for softer interactions and fcc for harder interactions, in qualitative agreement with our findings. The same trend is known for simple liquids with inverse power potentials.[31–34] The most direct comparison is possible with the computer simulations of the log-Yukawa potential by Watzlawek *et al.*[19] These authors obtained a phase diagram with exactly the same topology at low and intermediate densities. However, for large arm number the remelting is replaced by transitions to more ''exotic'' crystal structures at high densities: body-centered orthogonal (bco) and diamond lattices. A search for body-centered tetragonal (bct) and diamond crystals within the present theory produced no thermodynamically stable states. Especially the diamond lattice requires rather small nearest neighbor distances in the interesting density range, which is excluded by the following mechanism. When two neighboring sites come closer to each other the value of n_3 at their midpoint increases and eventually approaches unity, which

obviously induces a divergence of the functional. For high densities the differences between the log-hypergeometric and the log-Yukawa potential are expected to be small, as the logarithmic core dominates. We conclude that the absence of the exotic structures is a shortcoming of the theory. We did not attempt to determine the phase diagram by simulation since this would necessitate a large number of expensive free energy calculations. But the fcc crystal for $q=100$ is mechanically unstable for $\rho^*>1.76$, slightly above the theoretical remelting transition.

V. DISCUSSION

The proposal of a new DFT has to be accompanied by examples of successful use. As a meaningful application, one could choose a well-studied model, e.g., the inverse-power potentials (see, e.g., Refs. 31–34), and let the new candidate compete with established theories. We have postponed this necessary work and have tackled the star polymer system, which has a quite young history. Besides the technical advantage that we can calculate certain quantities analytically, this system is of great actual interest.

The strategy of the SFMT is to assume a generic form of a density functional and to impose the correct behavior in well-defined limiting cases. In its present form, the theory captures the virial expansion up to second order correctly, as well as a density distribution given by a single delta peak times an average occupation number which is called zero-dimensional limit. The theory has deficiencies: Two delta functions which are separated within the range of the pair interaction are not described exactly. In this respect the SFMT is in a poorer state than the hard sphere FMT, which describes even three delta spikes exactly.[5] Improving the SFMT along these lines is desirable; also Sweatman's work[35] and Percus' general rank two representation[36] should be useful.

We could show that the recent improvements in hard sphere FMT using tensorial weighted densities can (and need to) be done in SFMT to get a good description of the crystal. This situation is similar for hard spheres.[8,9,5] No empirical rescaling like in Ref. 14 was used in the present work in order to highlight the power of the approach and its deficiencies. The deficiencies occur at high density, where the star polymers freeze into exotic bco and diamond structures, that are not found to be stable within our approach. Nevertheless, intriguing high-density effects, like the broadening of density peaks upon increasing the density and remelting are described by SFMT. The sequence liquid–fcc–bcc–fcc upon increasing densities is correct. From the investigation of the star polymer model, we conclude that freezing, liquid and crystal properties of particles with soft interactions can be understood on the basis of a density functional that does not need input from the homogeneous fluid phase.

ACKNOWLEDGMENTS

Arben Jusufi is gratefully acknowledged for providing the simulation data in Fig. 1. We thank Bela Mulder for useful remarks. This work is part of the research program of the Stichting voor Fundamenteel Onderzoek der Materie. B.G. acknowledges financial support from the EU and from the Nederlandse Organisatie voor Wetenschappelijk Onderzoek.

[1] R. Evans, in *Fundamentals of Inhomogeneous Fluids*, edited by D. Henderson (Dekker, New York, 1992), p. 85.
[2] Y. Rosenfeld, Phys. Rev. Lett. **63**, 980 (1989).
[3] Y. Rosenfeld, M. Schmidt, H. Löwen, and P. Tarazona, J. Phys.: Condens. Matter **8**, L577 (1996); Phys. Rev. E **55**, 4245 (1997).
[4] P. Tarazona and Y. Rosenfeld, Phys. Rev. E **55**, R4873 (1997).
[5] P. Tarazona, Phys. Rev. Lett. **84**, 694 (2000).
[6] J. A. Cuesta, Phys. Rev. Lett. **76**, 3742 (1996).
[7] J. A. Cuesta and Y. Martinez-Raton, Phys. Rev. Lett. **78**, 3681 (1997).
[8] B. Groh and B. Mulder, Phys. Rev. E **61**, 3811 (2000).
[9] B. Groh, Phys. Rev. E **61**, 5218 (2000).
[10] C. Tutschka and G. Kahl, Phys. Rev. E **62**, 3640 (2000).
[11] M. Schmidt, J. Phys.: Condens. Matter **11**, 10163 (1999).
[12] Y. Rosenfeld, M. Schmidt, M. Watzlawek, and H. Löwen, Phys. Rev. E **62**, 5006 (2000).
[13] M. Schmidt, H. Löwen, J. Brader, and R. Evans, Phys. Rev. Lett. **85**, 1934 (2000).
[14] M. Schmidt, Phys. Rev. E **60**, R6291 (1999).
[15] M. Schmidt, Phys. Rev. E **62**, 4976 (2000).
[16] M. Schmidt, Phys. Rev. E **62**, 3799 (2000).
[17] C. N. Likos, H. Löwen, M. Watzlawek, B. Abbas, O. Jucknischke, J. Allgaier, and D. Richter, Phys. Rev. Lett. **80**, 4450 (1998).
[18] M. Watzlawek, H. Löwen, and C. N. Likos, J. Phys.: Condens. Matter **10**, 8189 (1998).
[19] M. Watzlawek, H. Löwen, and C. N. Likos, Phys. Rev. Lett. **82**, 5289 (1999).
[20] M. Watzlawek, ''Phase behavior of star polymers,'' Ph.D. thesis, University of Düsseldorf, 1999, published by Shaker Verlag, Aachen.
[21] A. Jusufi, M. Watzlawek, and H. Löwen, Macromolecules **32**, 4470 (1999).
[22] C. von Ferber, A. Jusufi, C. N. Likos, H. Löwen, and M. Watzlawek, Eur. Phys. J. E **2**, 311 (2000).
[23] R. Ohnesorge, H. Löwen, and H. Wagner, Europhys. Lett. **22**, 245 (1993).
[24] J. Stellbrink, B. Abbas, J. Allgaier, M. Monkenbusch, D. Richter, C. N. Likos, H. Löwen, and M. Watzlawek, Prog. Colloid Interface Sci. **110**, 25 (1998).
[25] C. N. Likos, H. Löwen, A. Poppe, L. Willner, J. Roovers, B. Cubitt, and D. Richter, Phys. Rev. E **58**, 6299 (1998).
[26] To convert the variables from Fig. 3(b) in Ref. 21 to the present ones, we divide the distances and multiply the forces by the same correction parameter, given as $2\lambda \exp((1+\sqrt{f}/2)^{-1}-(2q)^{-1}\ln(^{2q}_{q}))$, where λ is the ratio between the corona diameter σ^* and twice the radius of gyration. The actual values are $\lambda=0.68$, 0.66, 0.69 for $f=18$, 30, 50, respectively, as given in Table I of Ref. 21.
[27] J. Hansen and L. Verlet, Phys. Rev. **184**, 151 (1969).
[28] T. A. Witten, P. A. Pincus, and M. E. Cates, Europhys. Lett. **2**, 137 (1986).
[29] G. A. McConnell, A. P. Gast, J. S. Huang, and S. D. Smith, Phys. Rev. Lett. **71**, 2102 (1993).
[30] G. A. McConnell and A. P. Gast, Macromolecules **30**, 435 (1997).
[31] R. Agrawal and D. A. Kofke, Mol. Phys. **85**, 23 (1995).
[32] D. C. Wang and A. P. Gast, J. Phys.: Condens. Matter **11**, 10133 (1999).
[33] D. C. Wang and A. P. Gast, Phys. Rev. E **59**, 3964 (1999).
[34] D. C. Wang and A. P. Gast, J. Chem. Phys. **110**, 2522 (1999).
[35] M. B. Sweatman, ''Density functional theories of simple fluids and their mixtures,'' Ph.D. thesis, University of Bristol, 1995.
[36] J. K. Percus, J. Stat. Phys. **52**, 1157 (1988).